

# Spin-filtered Edge States with an Electrically Tunable Gap in a Two-Dimensional Topological Crystalline Insulator

Junwei Liu<sup>1,2</sup>, Timothy H. Hsieh<sup>2</sup>, Peng Wei<sup>2,3</sup>, Wenhui Duan<sup>1</sup>, Jagadeesh Moodera<sup>2,3</sup> and Liang Fu<sup>2\*</sup>

<sup>1</sup>*Department of Physics and State Key Laboratory of Low-Dimensional Quantum Physics, Tsinghua University, Beijing 100084, People's Republic of China*

<sup>2</sup>*Department of Physics, Massachusetts Institute of Technology, Cambridge, MA 02139*

<sup>3</sup>*Francis Bitter Magnet Lab, Massachusetts Institute of Technology, Cambridge, MA 02139*

Three-dimensional topological crystalline insulators were recently predicted and observed in the SnTe class of IV-VI semiconductors, which host metallic surface states protected by crystal symmetries. In this work, we study thin films of these materials and expose their potential for device applications. We demonstrate that thin films of SnTe and  $\text{Pb}_{1-x}\text{Sn}_x\text{Se}(\text{Te})$  grown along the (001) direction are topologically nontrivial in a wide range of film thickness and carry conducting spin-filtered edge states that are protected by the (001) mirror symmetry via a topological invariant. Application of an electric field perpendicular to the film will break the mirror symmetry and generate a band gap in these edge states. This functionality motivates us to propose a novel topological transistor device, in which charge and spin transport are maximally entangled and simultaneously controlled by an electric field. The high on/off operation speed and coupling of spin and charge in such a device may lead to electronic and spintronic applications for topological crystalline insulators.

PACS numbers:

Crystal structure and symmetry play a fundamental role in determining electronic properties of quantum materials. The interplay between crystallography and electronic topology[1, 2] has advanced our understanding of topological insulators[3–5]. More recently, a new type of topological phases termed topological crystalline insulators[6] has been predicted[7] and observed[8–10] in three-dimensional materials SnTe and  $\text{Pb}_{1-x}\text{Sn}_x\text{Se}(\text{Te})$ . A key characteristic of topological crystalline insulators is the presence of metallic boundary states that are protected by crystal symmetry, rather than time-reversal[11]. As a consequence, these states can acquire a band gap under perturbations that break the crystal symmetry[7, 12]. This novel property opens up an unprecedented possibility of tuning the charge and spin transport of topological boundary states with high on/off speed by applying an electric field. Here we theoretically demonstrate that thin films of SnTe and  $\text{Pb}_{1-x}\text{Sn}_x\text{Se}(\text{Te})$  grown along the (001) direction realize a new, two-dimensional topological crystalline insulator phase that supports spin-filtered edge states with a band gap tunable by electric field effect. Our work may thus enable electronic and spintronic device applications based on topological crystalline insulators.

Topological crystalline insulators (TCI) have so far only been realized in three-dimensional materials[7–10]. In this work, we propose a material realization of a two-dimensional (2D) topological crystalline insulator phase, which is topologically distinct from an ordinary insulator in the presence of mirror symmetry about the 2D plane.

The topology here is mathematically characterized by two integer topological invariants  $N_+$  and  $N_-$ , which are Chern numbers of Bloch states with opposite mirror eigenvalues. While the sum  $N_+ + N_-$  determines the quantized Hall conductance, the mirror Chern number[2] defined by  $N_M \equiv (N_+ - N_-)/2$  serves as an independent topological index[7, 13–17], which distinguishes a mirror-symmetric TCI in two dimensions.

The mirror eigenvalue of an electron wavefunction is intimately related to its spin. Because performing mirror transformation (denoted by  $M$ ) twice is equivalent to a  $2\pi$  rotation which changes the sign of a spinor,  $M^2 = -1$  and hence mirror eigenvalues are either  $i$  or  $-i$ . In the absence of spin-orbit coupling, these two eigenvalues correspond to spin eigenstates  $s_z = \pm \frac{1}{2}$  where the quantization axis  $z$  is perpendicular to the plane, so that mirror Chern number  $N_M$  reduces to spin Chern number[18–20]. More broadly, mirror Chern number can be defined for any system that is symmetric under reflection, with or without spin conservation. For instance, the quantum spin Hall state in graphene proposed by Kane and Mele[21] is characterized by  $|N_M| = 1$ , in addition to the  $Z_2$  index.

In this work, we demonstrate that (001) thin films of topological crystalline insulator SnTe and  $\text{Pb}_{1-x}\text{Sn}_x\text{Se}(\text{Te})$  in a wide range of thickness realize a 2D topological phase indexed by mirror Chern number  $|N_M| = 2$ , which supports *two* pairs of spin-filtered edge states[22]. This new topological phase belongs to a different symmetry class than the quantum spin Hall state, and its edge states are protected solely by mirror symmetry instead of time reversal. A *unique* consequence is that applying an electric field perpendicular to the film breaks the mirror symmetry and generates a band gap in these

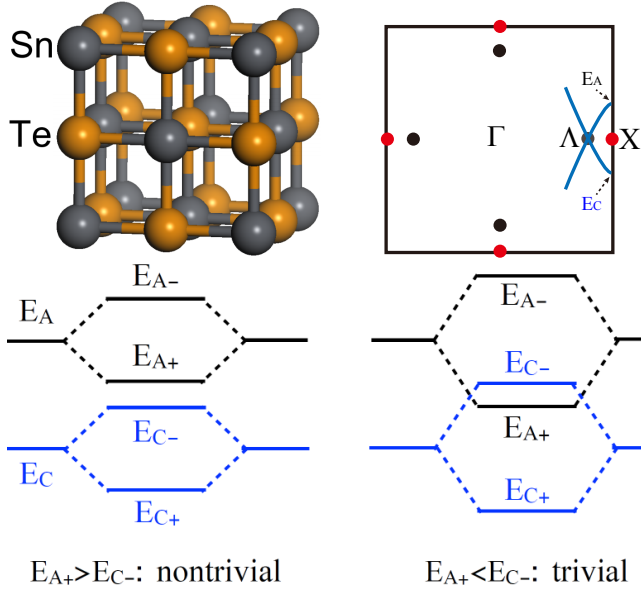


FIG. 1: Rocksalt structure of SnTe and schematic Brillouin zone of the 001 surface of three-dimensional SnTe. There are four massless Dirac points (indicated by the black dots). (bottom) Schematic conduction and valence bands of a TCI film at the  $X$  point. When the top and bottom surfaces hybridize weakly, the film inherits the inverted band gap of the 3D limit (left). Strong hybridization drives a band crossing, leading to a trivial phase (right).  $A, C$  denote anion/cation, and  $\pm$  denote bonding/anti-bonding combinations of the two surfaces.

edge states. This functionality leads to a new way of controlling the charge and spin transport simultaneously by electric field effect in a two-dimensional topological crystalline insulator.

Our results are based on a combination of  $k \cdot p$  modeling, band structure calculations, and topological band theory. A detailed derivation of the following analysis can be found in Methods. Here, we explain how competition between (1) the inverted band structure in the three-dimensional limit and (2) hybridization between the two surfaces determines the topological nature of the TCI film as a function of film thickness.

One of the hallmarks of a three-dimensional TCI, SnTe or  $\text{Pb}_{1-x}\text{Sn}_x\text{Se}(\text{Te})$ , are the four gapless Dirac points on the (001) surface. These are located at points  $\Lambda$  near the  $X$  points, and can in fact be derived from the  $k \cdot p$  theory at the  $X$  point [23]. We will see that it is the gapped states at  $X$  instead of the gapless states at  $\Lambda$  in the three-dimensional limit, which dictate the topological properties of the thin film. Surface states at  $X$  have energies  $E_C(X) = m$  and  $E_A(X) = -m$ , which are derived from the cation (C) and the anion (A) respectively. Importantly, TCI has an inherently inverted band ordering  $m < 0$  [7], with  $E_A(X)$  near the conduction band edge and  $E_C(X)$  near the valence band edge [26].

We now consider TCI (001) films with an odd number

of atomic layers, which are symmetric under the reflection  $z \rightarrow -z$  about the 2D plane in the middle [27] (see Fig. 1). SnTe and  $\text{Pb}_{1-x}\text{Sn}_x\text{Te}$  films have been epitaxially grown in a layer-by-layer mode with good thickness control [28–30]. When the film thickness is below the penetration length of surface states, the wavefunction hybridization between the top and bottom surfaces results in an energy splitting between the bonding and anti-bonding states. These hybridized surface states form the conduction and valence bands of the TCI film in the two-dimensional limit. Based on  $k \cdot p$  analysis (see Methods) and band structure calculations, we find that the conduction and valence bands of the TCI film at the  $X$  point are derived from the bonding state of the anion at energy  $E_{A+}(X)$  and the anti-bonding state of the cation at energy  $E_{C-}(X)$ . Due to their opposite parity, the two bands  $E_{A+}(X)$  and  $E_{C-}(X)$  do not repel each other. The band ordering of  $E_{A+}(X)$  and  $E_{C-}(X)$  depends on the competition between the hybridization of the two surfaces and the inverted gap  $2m$  of each surface. For thick films, the hybridization is weak so that  $E_{A+}(X) > E_{C-}(X)$ . With this ordering, the band structure of the TCI film is adiabatically connected to the original surface states in the three-dimensional limit, which is inherently inverted near  $X$  points (see Fig. 1).

We now concentrate on the band inversion near the transition point  $E_{A+}(X) \sim E_{C-}(X)$ , which occurs at a critical film thickness to be determined from band structure calculations later. This transition is described by Dirac mass reversal in a  $k \cdot p$  Hamiltonian:

$$H(\mathbf{k}) = (\tilde{v}_x k_x s_x - \tilde{v}_y k_y s_y) \tau_x + \tilde{m} \tau_z. \quad (1)$$

where  $\tau_z = \pm 1$  denotes the conduction and valence band of the TCI film at  $X$ , and each band has a Kramers degeneracy labelled by  $s_z$ . The velocities  $\tilde{v}_x, \tilde{v}_y$  and the Dirac mass  $\tilde{m} \equiv E_{C-}(X) - E_{A+}(X)$  are derived from microscopic parameters of surface states in the 3D TCI and their hybridization strengths (see Methods for details).

Importantly,  $H(\mathbf{k})$  is invariant under mirror symmetry about the 2D plane:

$$MH(\mathbf{k})M^{-1} = H(\mathbf{k}). \quad (2)$$

Here the mirror operator is given by  $M = -is_z \tau_z$ , because bonding and anti-bonding states have opposite mirror eigenvalues, and so are spin up and down states. For a single-flavor Dirac fermion, sign reversal of Dirac mass  $\tilde{m}$  changes mirror Chern number  $N_M$  by 1 [2]. We further take into account that there exist two  $X$  points in the Brillouin zone, related by a four-fold rotation. Because of the simultaneous band inversions at both  $X$  points,  $N_M$  changes by 2:

$$|N_M(\tilde{m} > 0) - N_M(\tilde{m} < 0)| = 2. \quad (3)$$

Combining this equation with the inverted band structure of  $\tilde{m} < 0$  deduced earlier, we conclude that

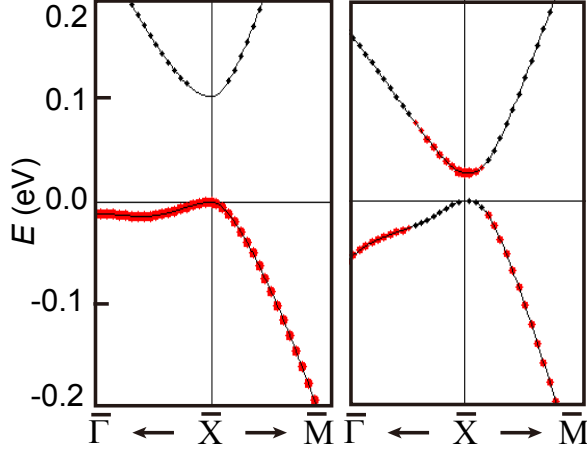


FIG. 2: Conduction and valence bands of a 3 layer (left) and 5 layer (right) SnTe film. Red dots denote the weight of the electronic wavefunction on the anion Te. The 5 layer film shows an inverted band structure relative to an ionic insulator.

(001) thin films of TCI with an inverted band ordering  $E_{A+}(X) > E_{C-}(X)$  realize a two-dimensional topological crystalline insulator phase with mirror Chern number  $|N_M| = 2$ .

The above conclusion drawn from  $k \cdot p$  analysis and topological band theory is confirmed by our band structure calculations of (001) TCI films based on a realistic tight-binding model[31], using SnTe as a representative. Fig.2 shows the band structures and orbital characters near the  $X$  point for 3- and 5-layer films. Clearly, the 5-layer film has an inverted band ordering with the conduction (valence) band near  $X$  derived from the anion (cation), while the 3-layer film does not. This confirms our  $k \cdot p$  result that the increased hybridization strength in thinner films drives the system out of the inverted regime. We further calculate the mirror Chern number numerically by integrating the Berry curvature over the Brillouin zone (see Methods), and confirm that  $N_M = 0$  for the 3-layer film and  $|N_M| = 2$  for the 5-layer film.

As the film thickness increases above 5 layers, the band gap at  $X$ ,  $E_g(X) \equiv E_{A+}(X) - E_{C-}(X)$  increases monotonically towards the value 220meV set by the band structure of a single surface. Meanwhile, the fundamental band gap in thicker films shifts from  $X$  to the momentum  $\Lambda$  located on the line  $\Gamma X$ . In the 3D limit, the gap at  $\Lambda$  goes to zero, thus recovering zero-energy Dirac points of TCI surface states (see Fig.3). Importantly, the nontrivial band topology is dictated by the inverted band structure at  $X$  instead of  $\Lambda$ , and thus stays present for SnTe films thicker than 5 layers. This leads to a robust 2D topological crystalline insulator phase in a *wide* range of thickness. The same holds for  $\text{Pb}_{1-x}\text{Sn}_x\text{Se}$  and  $\text{Pb}_{1-x}\text{Sn}_x\text{Te}$ , though the critical thickness for the non-trivial phase depends on material details. Moreover, the inverted gap in 11-layer SnTe film reaches 0.15eV near

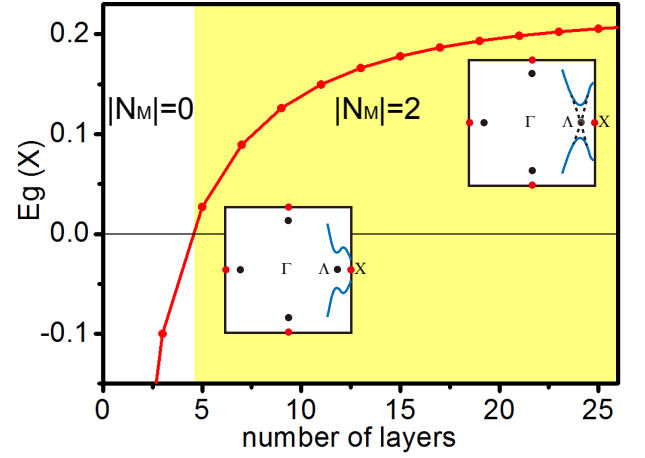


FIG. 3: Band gap of a TCI at the  $X$  point as a function of film thickness. Above five layers, the gap of SnTe at  $X$  is inverted and increases with thickness, resulting in a wide region of topologically nontrivial phase. For thick films, the fundamental band gap shifts from  $X$  to  $\Lambda$ , where the Dirac points of 3D surface states are located (insets).

the  $X$  point, which is much larger than that of existing quantum spin Hall insulators.

**Edge-state transport:** A hallmark of nontrivial band topology is the presence of conducting edge states. The mirror Chern number  $|N_M| = 2$  dictates that there exist two pairs of counter-propagating edge states within the band gap, and those moving in the same (opposite) direction carry identical (opposite) mirror eigenvalues. This is confirmed in our band structure calculation of a SnTe thin film in a strip geometry parallel to  $[100]$ , using the recursive Green's function method[33]. As shown in Fig. 4, edge states with opposite mirror eigenvalues cross each other at a pair of momenta in the edge Brillouin zone. In the ballistic limit, the conductance through such edge states is  $2e^2/h$ .

Unlike helical edge states in a quantum spin Hall insulator, the band crossings of spin-filtered edge states found here are located at *non*-time-reversal-invariant momenta, so that they are protected solely by the mirror symmetry  $z \rightarrow -z$  instead of time-reversal. This leads to a remarkable consequence: applying a perpendicular electric field, which breaks the mirror symmetry, will generate a band gap in these edge states. To illustrate this effect and estimate its magnitude, we calculate the band structure of an 11-layer SnTe film under a modest, uniform electric field that generates a 0.1eV potential difference across the film, and find that the spin-filtered edge states become completely gapped (see Fig.4). For comparison, a magnetic field or induced ferromagnetism is required to gap helical edge states of a quantum spin Hall insulator, which is difficult to achieve[34] and manipulate efficiently.

Thus edge-state transport in the 2D topological crystalline insulator phase found here has the unique prop-

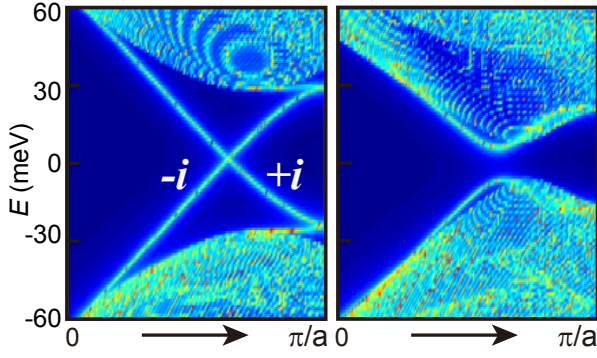


FIG. 4: Edge states of a TCI film and electric-field-induced gap. (Left) Bulk and gapless edge dispersion of a 11 layer SnTe film, labelled with mirror eigenvalues. (Right) Gapped dispersion when a perpendicular electric field is applied to generate a potential difference of 0.1eV across the film.

erty that the conductance is easily and widely tunable via an electric-field-induced gap instead of carrier depletion. This mechanism works at high on/off speed and improves power efficiency. As the on/off states originate from the crystal symmetry and symmetry breaking, they are more robust to material imperfections, which may also increase the operating cycles and improve the performance of the transistor especially at high frequency. The resistance of the “Off” state depends on the amount of impurity states inside the energy gap, and thus the On/Off ratio can be improved by controlling the film quality[35]. On the other hand, in the ballistic transport regime, the On/Off ratio of the topological transistor can be further enhanced with a quantized “On” state conductance of  $2e^2/h$  per edge and a negligible “Off” state conduction. Further, since electron spin is proportional to mirror eigenvalue, an electric current carried by the TCI edge states has a substantial out-of-plane spin polarization, and reversing the current flips the spin (Fig.5). This motivates us to propose a topological transistor device made of dual-gated TCI thin films, as shown in Fig.5. The device “On” state in Fig. 5 itself can be used as a spin diode that enables the electric field control of the electron spin polarization. Using the two gates, one can control the electric field across the film and the carrier density independently, and thus turn on and off the coupled charge and spin transport by purely electrical means functioning as a transistor.

In addition to an electric field, a magnetic field can also be applied to a TCI thin film to independently control the dispersion of the two sets of edge modes. Consider the (100) edge states with crossings at  $\pm k_0$ , and apply a magnetic field  $B = (B_{||}, B_{\perp}, B_z)$  (parallel being along the edge).  $B_z$  will shift both the energies and momenta of these crossings, while in-plane magnetic field  $B_{||}$  and  $B_z$  open up gaps. By tuning both electric and magnetic fields, the gaps at  $\pm k_0$  can be separately tuned in full

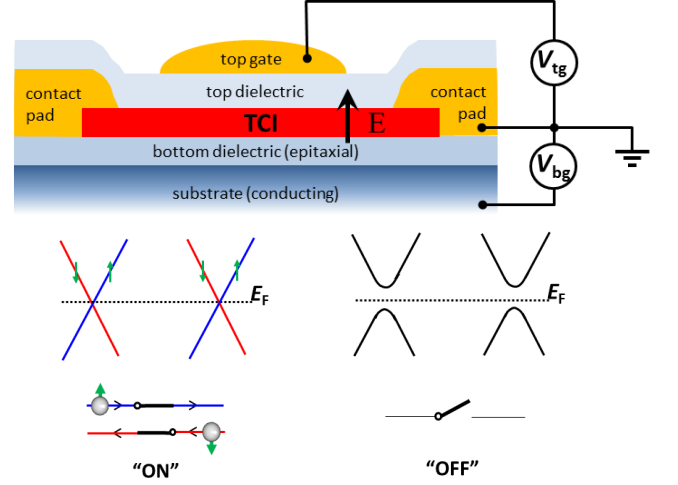


FIG. 5: Proposed topological transistor device for using an electric field to tune charge and spin transport. Without an electric field, the TCI film has mirror symmetry and thus protected, spin-filtered edge states (left). Applying an electric field perpendicular to the film breaks mirror symmetry, which gaps the edge states (right).

range:

$$\Delta_{k_0} = \sqrt{(m_E + m_{B_{\perp}})^2 + m_{B_{||}}^2} \quad (4)$$

$$\Delta_{-k_0} = \sqrt{(-m_E + m_{B_{\perp}})^2 + m_{B_{||}}^2}. \quad (5)$$

Here  $m_E, m_{B_{\perp}}, m_{B_{||}}$  are energy gaps that are generated separately from the corresponding fields (see Methods).

From the material standpoint, thin films of IV-VI semiconductors have been grown epitaxially[28–30] and extensively studied[36]. In particular, ultrathin SnTe quantum wells have been made with high quality[37–39]. Related materials PbTe, PbSe and PbS, while topologically trivial in bulk form, can become inverted in strained thin films[7], which further broadens the material base available for use. Ballistic transport with remarkable conductance quantization has been recently demonstrated in quantum devices based on IV-VI semiconductor quantum wells[40]. These developments as well as intensive interest in TCI thin films [41, 42] give us hope that the two-dimensional topological crystalline insulator phase and topological transistor device proposed here can be experimentally realized in the future.

## Methods:

### I. Derivation of $k \cdot p$ theory for TCI film

Here we provide the derivation leading up to the effective Hamiltonian (1). The starting point is (001) topological surface states of TCI in the three-dimensional limit. The  $k \cdot p$  Hamiltonian for these surface states, linearized

at an  $X$  point, is given by:

$$H_0(\mathbf{k}) = (v_x k_x s_y + v'_x k_x s_z \tau_x - v_y k_y s_x) \sigma_z + m \tau_z. \quad (6)$$

$\sigma_z = \pm 1$  denote the top/bottom (001) surfaces,  $\tau_z = 1(-1)$  denote basis states that are mainly derived from the cation(anion), and  $s_z = \pm 1$  denotes a Kramers doublet. For a given value of  $\sigma_z$ ,  $H_0(\mathbf{k})$  reduces to the four-band  $k \cdot p$  Hamiltonian for a single surface, derived in Ref.[23–25]. Note, however, for technical convenience, we have chosen a basis different from that in Ref.[23], such that  $H_0(\mathbf{k}=0)$  is diagonal.

$H_0(\mathbf{k})$  is invariant under the symmetry operations of inversion  $P$ ,  $M_z : z \rightarrow -z$ ,  $M_x : x \rightarrow -x$ ,  $M_y : y \rightarrow -y$ , two-fold rotation about  $z$ -axis  $C_2$ , and time-reversal  $\Theta$ . In the above basis, these are represented by

$$\begin{aligned} P &= \sigma_x, \\ M_z &= -i s_z \tau_z \sigma_x, \\ M_x &= -i s_x, \\ M_y &= -i s_y \tau_z, \\ C_2 &= -i s_z \tau_z, \\ \Theta &= i s_y K. \end{aligned} \quad (7)$$

Hybridization between the two surfaces corresponds to off-diagonal terms in  $\sigma_z$  basis. There are three hybridization terms allowed by the above symmetries:

$$H_h(\mathbf{k}) = \delta_1 \sigma_x + \delta'_1 \tau_z \sigma_x + \delta_2 s_x \tau_y \sigma_x. \quad (8)$$

Here  $\delta_1 \pm \delta'_1$  is the intra-orbital hybridization matrix element within the cation (anion) orbitals on the top and bottom surface.  $\delta_2$  is the inter-orbital hybridization matrix element between the cation and anion orbitals on the two surfaces. By combining (6) and (8), we obtain an eight-band  $k \cdot p$  Hamiltonian for the (001) thin film of TCI:

$$H_t(\mathbf{k}) = H_0(\mathbf{k}) + H_h(\mathbf{k}). \quad (9)$$

The intra-orbital hybridization  $\delta_1$  and  $\delta'_1$  splits a pair of degenerate states at  $X$  on the two surfaces,  $E_{\alpha=C,A}(X)$ , into a bonding and anti-bonding states with energies  $E_{\alpha+}(X)$  and  $E_{\alpha-}(X)$  respectively. From band structure calculations, we find that  $\delta'_1$  is smaller than  $\delta_1$ , so that the bonding states have a lower energy than the anti-bonding states:  $E_{\alpha+}(X) < E_{\alpha-}(X)$ . In this case, the conduction and valence band edges at  $X$  are derived from the bonding combination of the anions at energy  $E_{A+}(X)$  and the anti-bonding orbital of the cations at energy  $E_{C-}(X)$ .

The transition as these two levels cross each other can be derived by projecting  $H_t(\mathbf{k})$  into the low-energy subspace of  $E_{A+}(X)$  and  $E_{C-}(X)$ . We find that  $\delta'_1$  plays an insignificant role and can be set to zero for simplicity. Projecting onto the four bands yields the  $k \cdot p$  Hamiltonian for TCI film, Eq.(1)

$$H(k) = \tilde{m} \tau_z + (\tilde{v}_x k_x s_x - \tilde{v}_y k_y s_y) \tau_x. \quad (10)$$

where the parameters are given by

$$\begin{aligned} \tilde{m} &= \sqrt{m^2 + \delta_2^2} - |\delta_1|, \\ \tilde{v}_x &= v'_x \text{sgn}(\delta_1 \delta_2), \\ \tilde{v}_y &= \frac{v_y |\delta_2|}{\sqrt{m^2 + \delta_2^2}}. \end{aligned} \quad (11)$$

## II. $k \cdot p$ theory for edge states

We now derive the  $k \cdot p$  theory of the gapless edge states, in order to analyze how they are affected by external fields. Note that above, the  $x$  direction is actually (110) with respect to crystal axes. Let us now choose  $x$  to be (100) and analyze the gapless edge states with crossings at  $\pm k_0$  along this axis.

The two symmetries that fix a single valley are  $M_z$  and  $M_x \Theta$ , and we choose the representation

$$M_z = -i s_z \quad (12)$$

$$M_x \Theta = i s_z K. \quad (13)$$

The following table denotes how the electric field  $E$  (in the  $z$  direction) and magnetic field  $(B_x, B_y, B_z)$  transforms under the two symmetries:

	$M_z$	$M_x \Theta$
$E$	$-$	$+$
$B_x$	$-$	$-$
$B_y$	$-$	$+$
$B_z$	$+$	$+$

The most general  $k \cdot p$  Hamiltonian compatible with the above is

$$\begin{aligned} H_{k_0}(k) &= v k s_z + m_E s_y + m_{B_{||}} s_x + m_{B_{\perp}} s_y \\ &\quad + E_{B_z} + E'_{B_z} s_z \end{aligned} \quad (14)$$

where  $v$  is velocity of edge states,  $m_E, m_{B_{||}}, m_{B_{\perp}}, E_{B_z}$  and  $E'_{B_z}$  are linearly proportional to the corresponding electric/magnetic field. Using time-reversal symmetry, we obtain the  $k \cdot p$  Hamiltonian for the other valley at  $-k_0$ :

$$\begin{aligned} H_{-k_0}(k) &= v k s_z - m_E s_y + m_{B_{||}} s_x + m_{B_{\perp}} s_y \\ &\quad - E_{B_z} + E'_{B_z} s_z \end{aligned} \quad (15)$$

By diagonalizing Eq.(14) and (15), we derive the field-induced gap (4) and (5) at the two valleys.

*Acknowledgement:* This work is supported by the U.S. Department of Energy, Office of Basic Energy Sciences, Division of Materials Sciences and Engineering under Award DE-SC0010526. T.H. acknowledges support under NSF Graduate Research Fellowship No. 0645960. J.L and W.D. acknowledge support from the Ministry of Science and Technology of China (Grant

Nos. 2011CB921901 and 2011CB606405) and the National Natural Science Foundation of China (Grant No. 11074139). P.W. and J. S. M. would like to thank support from the MIT MRSEC through the MRSEC Program of the NSF under award number DMR-0819762, as well as NSF DMR grants 1207469 and ONR grant N00014-13-1-0301. All correspondence should be addressed to L.F.

---

\* Electronic address: liangfu@mit.edu

- [1] L. Fu and C. L. Kane, Phys. Rev. B **76**, 045302 (2007).
- [2] J. Y. C. Teo, L. Fu and C. L. Kane, Phys. Rev. B **78**, 045426 (2008).
- [3] M. Z. Hasan and C. L. Kane, Rev. Mod. Phys. **82**, 3045 (2010).
- [4] X. L. Qi and S. C. Zhang, Rev. Mod. Phys. **83**, 1057 (2011).
- [5] J. E. Moore, Nature **464**, 194 (2010).
- [6] L. Fu, Phys. Rev. Lett. **106**, 106802 (2011).
- [7] T. H. Hsieh, H. Lin, J. Liu, W. Duan, A. Bansil and L. Fu, Nat. Commun. **3**, 982 (2012).
- [8] Y. Tanaka *et al.*, Nat. Phys. **8**, 800 (2012).
- [9] P. Dziawa *et al.*, Nat. Mat. **11**, 1023 (2012).
- [10] S. Xu *et al.*, Nat. Commun. **3**, 1192 (2012).
- [11] R. S. K. Mong, A. M. Essin, and J. E. Moore, Phys. Rev. B **81**, 245209 (2010).
- [12] Y. Okada *et al.*, Science, 29 August 2013 (10.1126/science.1239451).
- [13] R. Takahashi and S. Murakami, Phys. Rev. Lett. **107**, 166805 (2011).
- [14] M. Kargarian and G. A. Fiete, Phys. Rev. Lett. **110**, 156403 (2013).
- [15] C. -K. Chiu, H. Yao and S. Ryu, arXiv:1303.1843
- [16] T. Morimoto and A. Furusaki, arXiv:1306.2505
- [17] M. Ye, J. W. Allen and K. Sun, arXiv:1307.7191
- [18] D. A. Abanin, P. A. Lee and L. S. Levitov, Phys. Rev. Lett. **96**, 176803 (2006).
- [19] A. F. Young, J. D. Sanchez-Yamagishi, B. Hunt, S. H. Choi, K. Watanabe, T. Taniguchi, R. C. Ashoori, P. Jarillo-Herrero, arXiv:1307.5104
- [20] P. Maher, *et al.* Nature Physics **9**, 154158 (2013).
- [21] C. L. Kane and E. J. Mele, Phys. Rev. Lett. **95**, 226801 (2005); *ibid.* **95**, 146802 (2005).
- [22] J. Liu, T. H. Hsieh, W. Duan, J. Moodera and L. Fu, APS March Meeting (2013), <http://meetings.aps.org/link/BAPS.2013.MAR.J13.5>
- [23] J. Liu, W. Duan and L. Fu, arXiv:1304.0430
- [24] C. Fang, M. J. Gilbert, S. -Y. Xu, B. A. Bernevig and M. Z. Hasan, arXiv:1212.3285
- [25] Y. J. Wang, W.-F. Tsai, H. Lin, S. -Y. Xu, M. Neupane, M. Z. Hasan, A. Bansil, Phys. Rev. B **87**, 235317 (2013).
- [26] S. Safaei, P. Kacman and R. Buczko, Phys. Rev. B **88**, 045305 (2013).
- [27] Edge states are also present in TCI films with an even number of layers, whose protection involves a different symmetry to be described elsewhere.
- [28] G. Bauer and G. Springholz, Phys. Stat. Sol. (b), **244**, 2752 (2007).
- [29] E. Abramof, S. O. Ferreira, P. H. O. Rappl, H. Closs, and I. N. Bandeira, J. Appl. Phys. **82**, 2405 (1997).
- [30] A. Ishida, T. Yamada, T. Tsuchiya, Y. Inoue, S. Takaoka, and T. Kita, Appl. Phys. Lett. **95**, 122106 (2009).
- [31] C. S. Lent, M. A. Bowen, J. D. Dow, R. S. Allgaier, O. F. Sankey and E. S. Ho, Superlattices Microstruct. **2**, 491 (1986).
- [32] C. X. Liu, *et al.*, Phys. Rev. B **81**, 041307(R) (2010).
- [33] M. P. Lopez Sancho *et al.*, J. Phys. F: Met. Phys. **15** (1985).
- [34] L. Du, I. Knez, G. Sullivan and R. Du, arXiv:1306.1925
- [35] M. Lang *et al.*, Nano. Lett. **13**, 48 (2013).
- [36] D. Khokhlov, "Lead Chalcogenides: Physics and Applications", CRC Press (2002).
- [37] A. Ishida, M. Aoki, and H. Fujiyasu, J. Appl. Phys. **58**, 1901 (1985).
- [38] E. I. Rogacheva, O. N. Nashchekina, A. V. Meriuts, S. G. Lyubchenko, M. S. Dresselhaus and G. Dresselhaus, Appl. Phys. Lett. **86**, 063103 (2005).
- [39] A. A. Taskin, S. Sasaki, K. Segawa, and Y. Ando, arXiv:1305.2470
- [40] G. Grabecki *et al.*, Physica E, **34**, 560. (2006)
- [41] C. Fang, M. J. Gilbert, and B. A. Bernevig, arXiv:1306.0888.
- [42] Fan Zhang, Xiao Li, Ji Feng, C. L. Kane, and E. J. Mele, arXiv:1309.7682.